ЖЭТФ, 2013, том 143, вып. 1, стр. 191–197

STRUCTURAL, ELECTRICAL, AND THERMOELECTRICAL PROPERTIES OF $(Bi_{1-x}Sb_x)_2Se_3$ ALLOYS PREPARED BY A CONVENTIONAL MELTING TECHNIQUE

E. Kh. Shokr, E. M. M. Ibrahim*, A. M. Abdel Hakeem, A. M. Adam

Physics Department, Faculty of Science, Sohag University
82524, Sohag, Egypt

Received June 18, 2012

Polycrystalline solid solutions of $(Bi_{1-x}Sb_x)_2Se_3$ ($x = 0$, 0.025, 0.050, 0.075, 0.100) were prepared using a facile method based on the conventional melting technique followed by annealing process. X-ray analysis and Raman spectroscopical measurements revealed formation of Bi_2Se_3 in single phase. The electrical and thermoelectric properties have been studied on the bulk samples in the temperature range 100–420 K. The electrical conductivity measurements show that the activation energy and room-temperature electrical conductivity dependences on the Sb content respectively exhibit minimum and maximum values at $x = 0.05$. The thermoelectric power exhibited a maximum value near the room temperature suggesting promising materials for room-temperature applications. The highest power factor value was found to be 13.53 $\mu W \cdot K^{-2} \cdot cm^{-1}$ and recorded for the $x = 0.05$ compound.

DOI: 10.7868/S0044451013010191

1. INTRODUCTION

Thermoelectric materials have attracted the efforts of many research groups worldwide due to the wide applications ranging from a green power source to photon sensing devices. These materials can transform the temperature gradient to electric power or vice versa according to the Seebeck effect or the Peltier effect. They are regarded as sources of green power, where they use all kinds of energy such as waste heat, solar energy, radiant heat, etc. Furthermore, thermoelectric materials are reliable energy converters and have no environmentally harmful fluids, noise or vibrations, because there are no mechanical moving parts. Devices based on this technology can be manufactured in very small sizes, which enable application to localized areas with precise temperature control [1, 2]. Among all thermoelectric materials, narrow-band layered semiconducting solid solutions with $A_2^V B_3^{VI}$ of the tetradymite structure (where A is Bi or Sb and B is Se or Te) find various applications in the field of thermoelectric devices [3], which makes them interesting for both theoretical and applied investigations [4–8].

The efficiency of a thermoelectric power material can be evaluated by its power factor. Because it is expressed as $P = S^2\sigma$, where S is the Seebeck coefficient and σ is the electrical conductivity, it is a carrier-concentration-dependent factor [9, 10]. Intensive studies have been performed on the effect of doping on the bismuth selenide material. Because it is a narrow-gap semiconductor, its doping with certain impurities results not only in controlling the free carrier concentration but also in the appearance of a range of strong unusual properties that are not characteristic for the undoped material itself [11–16]. For example, doping Bi_2Se_3 by some IIIA elements such as In or Tl increases the power factor by as much as 25 % [11–13]. Furthermore, according to Ref. [14], a crossover of the Seebeck coefficient sign occurs for Bi_2Se_3 material by incorporation of Pb at a high level.

This paper presents a facile method for preparing Sb-doped Bi_2Se_3 alloys. A study on the effect of the Sb content on structural, electrical, and thermoelectric properties has been carried out with the aim to find the optimum doping level that gives the highest power factor. The preparation method based on the conventional melting method offers the advantages of a simple, inexpensive and successful technique for preparing polycrystalline materials with single phase. The

*E-mail: e.ibrahim@science.sohag.edu.eg

prepared samples were investigated by X-ray diffraction (XRD), Raman spectroscopy, scanning electron microscopy (SEM), and energy dispersive X-ray spectroscopy analyses (EDXA) in order to identify the microstructure, surface morphology, and stoichiometry.

2. EXPERIMENTAL

The polycrystalline alloys under investigation were prepared from high-purity (99.99 %) powder elements from Aldrich. The alloys were formed by melting the mixture of the pure elements at 1000 °C in a silica tube sealed under vacuum (10^{-5} Torr). The melting duration was 24 h with frequent agitation to ensure the complete homogeneous mixing. The melted mixtures were then cooled by furnace cooling at room temperature. After that, the silica tubes were broken and each ingot was grounded thoroughly for 1 h to obtain fine particles. The powder of each composition was pressed under 5 ton/cm^2 to shape it into a pellet and finally polished to be optically flat. The pellets were annealed at 150 °C for 4 h. The internal microstructure of the $(Bi_{1-x}Sb_x)_2Se_3$ ($0 \le x \le 0.10$) system was characterized by XRD (Brucker Axs-D8 Advance diffractometer with CuK_α radiation at $\lambda = 1.5406$ Å) and SEM (FEI NOVA NANOSEM-200 with the acceleration voltage equal to 15 kV) combined with an energy dispersive X-ray (EDX) spectrometer.

The resonance of Raman spectra at the excitation wavelength 532 nm was obtained using a Thermo Scientific DXR Smart Raman and Bruker FT RFS 100/s spectrometer. The electrical and thermoelectric measurements have been carried out using specially made sample holders. The dc electrical conductivity was measured by the four-probe method. For the thermoelectric power measurement, the sample was inserted between two parallel and highly polished copper electrodes. The ambient temperature and temperature gradient in the thermoelectric measurements were measured using standard copper–constantan thermocouples. The voltages and currents were measured using Keithly sensitive digital multimeters. All measurements were performed in the temperature range 100–420 K in a 10^{-3}-mmHg vacuum.

3. RESULTS AND DISCUSSION

The XRD patterns of $(Bi_{1-x}Sb_x)_2Se_3$ ($x = 0$–0.10) compounds are shown in Fig. 1. The data imply that the preparation method is appropriate for obtaining a single-phase structure where all peaks can be indexed to the pure hexagonal phase of Bi_2Se_3, with the unit cell parameters $a = 4.13960$ Å and $c = 28.63600$ Å

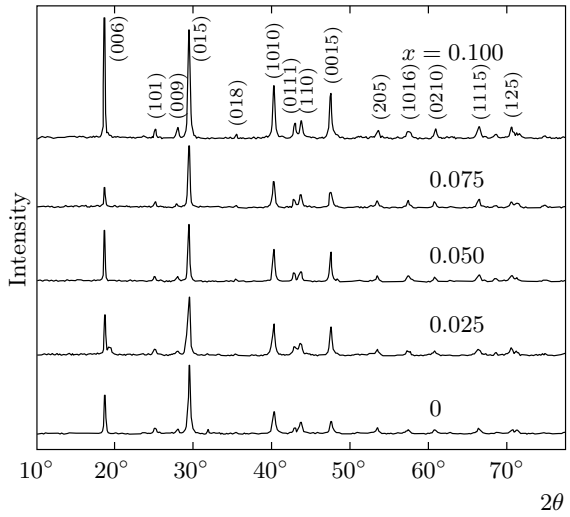

Fig. 1. XRD patterns for $(Bi_{1-x}Sb_x)_2Se_3$ ($x = 0$–0.10) samples

(space group: $R-3m$) [17]. The polycrystalline nature of the samples is clearly observed from the sharpness of the structural peaks. Notably, no indications of peaks corresponding to other Bi–Se compounds were detected. Also, the diffractograms of the Sb-doped samples do not exhibit any diffraction peaks of the ternary compounds of Bi_xSb_ySe. This may be attributed to the substitution of Bi ions by Sb ions and the resultant SbSe system crystallization into the same kind of structure. Furthermore, the ternary compound formation requires low cooling rate, high synthetic pressure, and high dopant concentration [18], which are not realized in this work.

The crystallite size D was calculated using the well-known Scherrer equation [19]

$$D = \frac{K\lambda}{\beta \cos\theta}, \qquad (1)$$

where λ is the wavelength of the X-rays, β is the full width at half maximum of the peak, θ is the Bragg angle, and K is the shape factor. The calculated values were in the range 63.1–104 nm.

The morphology of the prepared samples was investigated using the SEM. The micrographs depicted in Fig. 2 reveal that the grain size is variable and obviously decreases with antimony addition to reach the near-submicron scale. The final product composition was further investigated by the EDX (see the inset in Fig. 2). Noteworthy, analyzing different grains of each sample indicates that they are indeed of the same chemical composition, which implies good homogeneity of

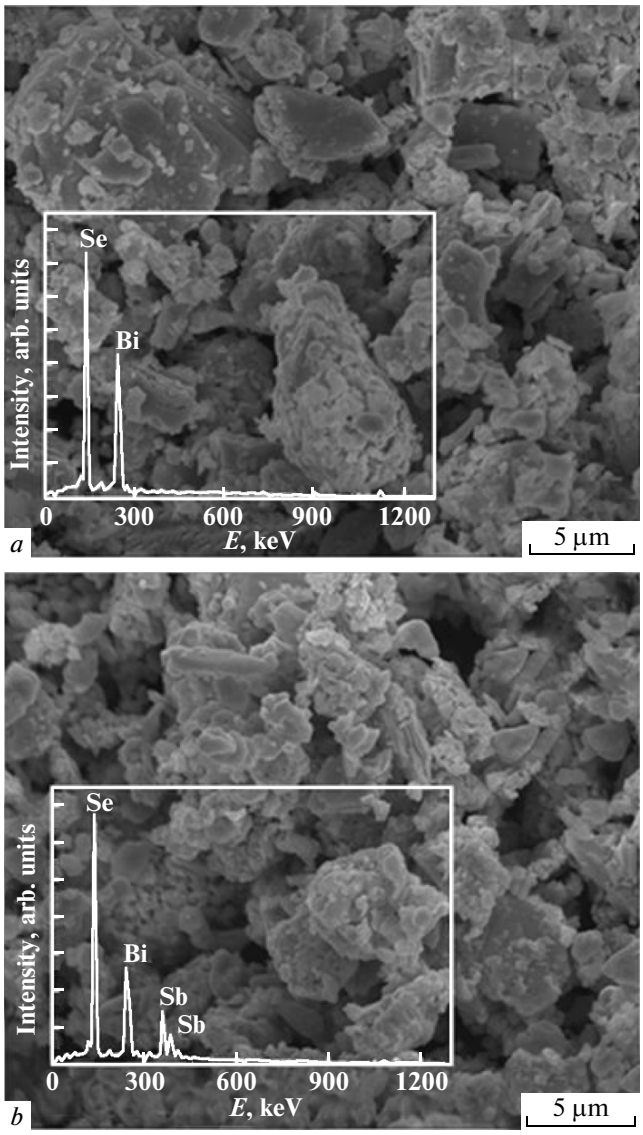

Fig. 2. SEM micrographs for $(Bi_{1-x}Sb_x)_2Se_3$ samples with (a) $x = 0$ and (b) $x = 0.10$. The insets show EDX analysis results

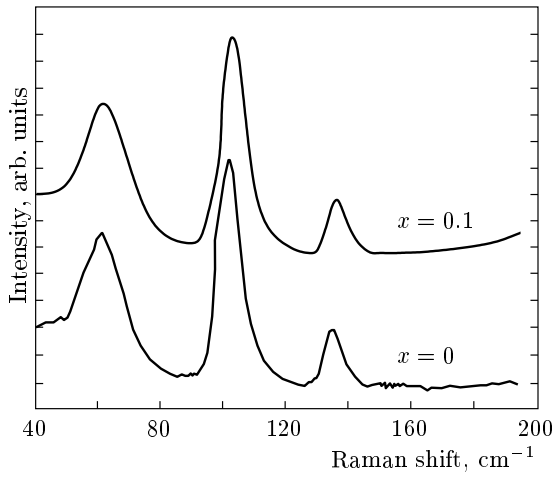

Fig. 3. Raman spectra for $x = 0$ and $x = 0.1$ samples

the prepared samples. The data tabulated in the Table suggest that all the $(Bi_{1-x}Sb_x)_2Se_3$ compositions possess superstoichiometry for the Bi element, which is normal for the Bi_2Se_3 compounds and attributed to evaporation of the Se content during the melting process [20]. The superstoichiometry of Bi element significantly affects the conduction of the compositions, as has been discussed above.

To obtain a deeper insight into the internal structure of the prepared solid solutions, Raman spectroscopy analyses were carried out. We note that no significant differences were observed between the Raman spectra of all the $Bi_{2-x}Sb_xSe$ samples under study. Consequently, only the Raman spectra corresponding to $x = 0$ and $x = 0.1$ samples are presented as examples in Fig. 3. It is well known that Bi_2Se_3 has a centrosymmetric rhombohedral structure that has a unit cell with one Se atom located in the $3a$ Wyckoff position and the remaining Bi(2) and Se(2) atoms occupying $6c$ Wyckoff sites. Hence, Bi_2Se_3 has ten zone-center modes at the Γ point of the Brillouin zone, which are expressed in terms of irreducible representation as [21]

$$\Gamma_{10} = 2A_{1g} + 3A_{2u} + 2E_g + 3E_u.$$

The g modes are Raman active, whereas the u modes are infrared active. The E_g modes correspond to atomic vibrations in the plane of the layers, while the A_{1g} modes correspond to vibrations along the c axis perpendicular to the layers [22, 23]. Therefore, bulk crystalline Bi_2Se_3 commonly exhibits four modes [23, 24]: E_g^1, A_{1g}^1, E_g^1, and A_{1g}^2, which respectively appear around 40, 61, 102, and 134 cm^{-1}. For our samples, formation of Bi_2Se_3 crystals is proved through appearance of three Raman-active modes at 61, 102, and 134 cm^{-1}. The E_g mode expected to be close to 40 cm^{-1} has not been observed (see Fig. 3), and it was also not seen in previously reported results [23, 24].

To examine electrical properties and conduction mechanisms, the dc electrical conductivity σ was measured as a function of the ambient temperature T in the temperature range 100–420 K. The σ–T plots illustrated in Fig. 4 suggest that the conduction mechanism in the lower temperature range of measurements ($T \leq T_\sigma$) is predominantly governed by the carrier scat-

Table. Bi, Sb, and Se contents determined using an EDX analysis and values of T_m, E_{s1}, and E_{s2} for $(Bi_{1-x}Sb_x)_2Se_3$ ($x = 0$–0.1) samples

Composition	Bi, at. %	Sb, at. %	Se, at. %	T_m, K	E_{s1}, eV	E_{s2}, eV
$x = 0$	42.20	–	57.80	300	0.02210	0.15463
$x = 0.025$	41.56	0.98	57.46	300	0.00654	0.02464
$x = 0.050$	40.90	2.09	57.01	230	0.01090	0.02050
$x = 0.075$	38.91	3.69	57.40	230	0.01201	0.05455
$x = 0.100$	37.78	4.60	57.62	220	0.00740	0.01653

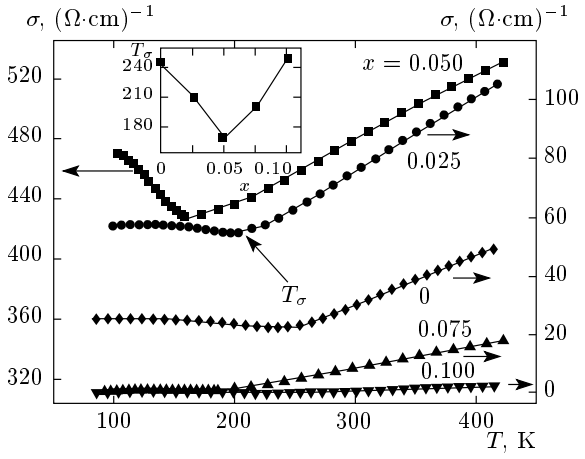

Fig. 4. Temperature dependences of the electrical conductivity for $(Bi_{1-x}Sb_x)_2Se_3$ ($x = 0$–0.1) samples. Inset is the Sb content dependence of the transition temperature T_σ

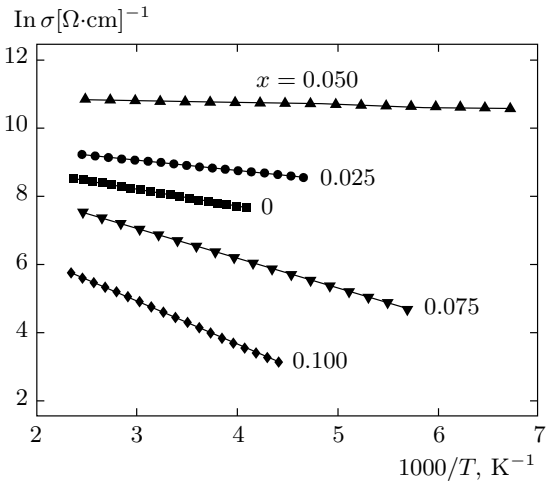

Fig. 5. The plots of $\ln\sigma$ versus $1000/T$ for $(Bi_{1-x}Sb_x)_2Se_3$ samples with different concentrations of the Sb content

tering processes [25–28]. It is worth noting that the temperature T_σ depends on the composition itself, as can be seen in the inset in Fig. 4. Above T_σ (in the higher temperature region), where the number of thermally excited carriers begins to overwhelm the number of carriers due to ionized impurities, the intrinsic conduction begins to dominate [29]. The temperature dependence of the electrical conductivity in the intrinsic region matches well with the relation

$$\sigma = \sigma_0 \exp\left(-\frac{\Delta E}{k_B T}\right), \qquad (2)$$

where σ_0 is the pre-exponential factor representing the temperature-independent conductivity, ΔE is the energy gap for the electrical conduction, and k_B is the Boltzmann constant. The plots of $\ln\sigma$ versus $1000/T$ for $(Bi_{1-x}Sb_x)_2Se_3$ samples in the semiconducting behavior range ($T \geq T_\sigma$) are shown in Fig. 5. The linear behavior of the plots confirms the thermally activated

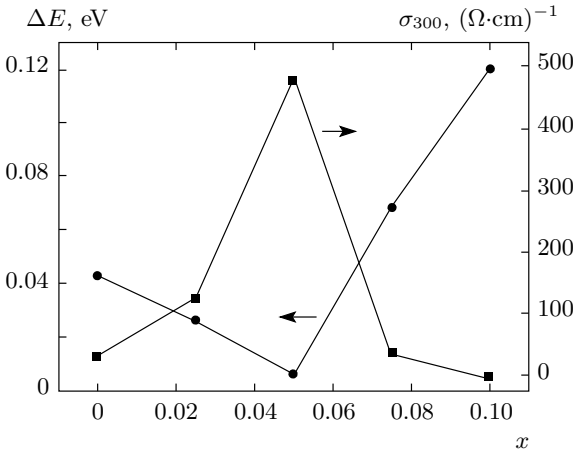

Fig. 6. Variation of the activation energy ΔE and room-temperature electrical conductivity σ_{300} with the antimony content for $(Bi_{1-x}Sb_x)_2Se_3$ samples

conduction. The ΔE values were determined and represented as functions of the doping content in Fig. 6. As we can see, ΔE decreases with increasing the doping content, exhibiting a minimum at $x = 0.05$ and then increases to have a maximum with the highest doping level. In the same figure, we can observe that the room-temperature electrical conductivity σ_{300} dependence on the antimony content behaves oppositely: it increases to a maximum at $x = 0.05$ and then decreases dramatically. The behavior of σ_{300} with the Sb content increase can be explained by invoking the ordering effect in the solid solution structure and the influence of bismuth superstoichiometry and the Sb content on the character and concentration of lattice point defects in the $(Bi_{1-x}Sb_x)_2Se_3$ crystal lattice. The superstoichiometric bismuth content in the undoped Bi_2Se_3 crystals gives rise to the n-type electrical conduction behavior due to the presence of positively charged vacancies in the selenium sublattice [30]. The excess of Bi in the crystal also results in formation of antisite defects (having negative charge) in the lattice due to replacing the selenium atoms in their lattice sites by bismuth atoms. It is reported in Ref. [20] that at a low Sb content, the free-electron concentration increases due to the occurrence of the uncharged substitution defects of antimony atoms in bismuth sites, which suppress the concentration of the antisite defects. But the decrease in the electron concentration in the region of a higher antimony content is due to the associated decrease in the concentration of the Se vacancies in the Se sublattice.

To calculate the power factor and thus check the feasibility of our compositions as thermopower materials, it is essential to carry out thermoelectric power measurements. The temperature dependence of the Seebeck coefficient S was measured in the same temperature range of the electrical conductivity measurements in order to obtain the optimum temperature that gives the higher power factor. As shown in Fig 7, in the entire temperature range considered, the value S is negative, exhibiting the domination of the conducting behavior of n-type semiconductors. The most characteristic for the bismuth selenide-based compounds is the n-type [31], but the p-type is also reported [16, 31, 32]. The modulus of S was found to increase as the temperature increases, reaching a maximum at a certain temperature T_m. Beyond this temperature, S decreases continuously with increasing the temperature. This temperature dependence of S confirms the transition to the intrinsic conduction discussed above, where the slope changes from positive to negative [33]. The largest modulus of the Seebeck coefficient was observed for the undoped sample, where S has the value 0.280 mV/K

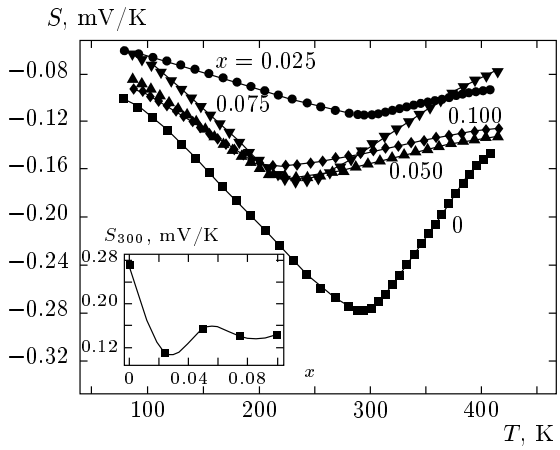

Fig. 7. Temperature dependences of the Seebeck coefficient for $(Bi_{1-x}Sb_x)_2Se_3$ ($x = 0$–0.1) samples. Inset is the Sb-content dependence of the room-temperature Seebeck coefficient S_{300}

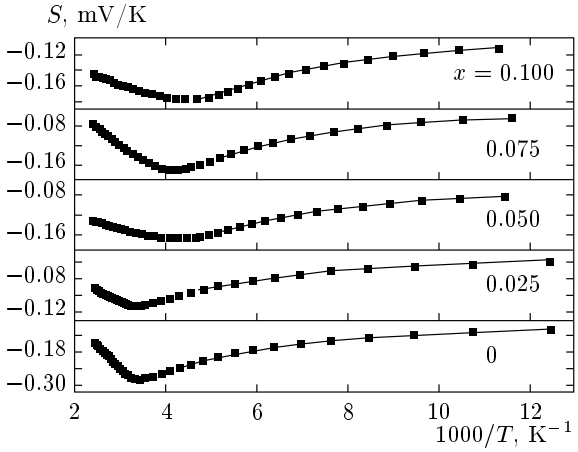

Fig. 8. Seebeck coefficient versus $1000/T$ for $(Bi_{1-x}Sb_x)_2Se_3$ ($x = 0$–0.1) samples

at $T = 300$ K. The inset in Fig. 7 clarifies a minimum value of the Seebeck coefficient for the $x = 0.025$ sample. However, at high doping levels ($x = 0.05$–0.10), no significant change of the S value can be observed.

For all samples, the temperature dependence of the Seebeck coefficient fits well with the following equation in the entire temperature range below and above the transition temperature:

$$S = \pm\frac{k_B}{e}\left(\frac{E_s}{k_B T} + A\right), \tag{3}$$

the activation energy E_s represents the thermopower activation energy and A is a dimensionless parameter related to the carrier scattering mechanisms or assumed

to be a measure of the kinetic energy transported by carriers. As can be seen in Fig. 8, the plots of S versus $1000/T$ consist of two linear segments. In the low-temperature region, the temperature dependence of S exhibits a smooth trend that reverses the smooth decrease in the charge carrier mobility with increasing temperature [34]. By contrast, above T_m, S changes rapidly with temperature, which may be attributed to the effective contribution of the p-type defect creation at high temperatures [35]. This behavior implies that the conduction is not of a pure n-type but is of a mixed type and the positive-charge carriers (holes) make a significant contribution. The transition temperature T_m and the thermopower activation energies E_{s1} and E_{s2} respectively corresponding to the temperature ranges below and above T_m for all samples are tabulated in the Table. The difference that could be observed between T_σ and T_m at transition temperatures for the same sample can be attributed to the difference in the electrical conductivity and thermoelectric power sensitivity to the defects included in the sample. The values of the thermopower and electrical conductivity activation energies E_{s2} and ΔE, are comparable. This demonstrates the absense of temperature-activated mobility and confirms the gap band conduction mechanism of charge transport in the high-temperature range, where $E_{s2} = \Delta E$ is the energy associated with carrier generation only. The small value of the thermopower activation energy E_{s1} in the low-temperature range is evidence of the domination of the temperature-activated mobility mechanism of conduction [36, 37] and matches well with the electrical conductivity results mentioned above.

The power factor P of a material is a good indicator of the performance of this material as a thermoelectric device. The higher the power factor of a material, the more useful it is as a thermoelectric material. Increasing the power factor value required large electrical conductivity and high thermoelectric power. Figure 9 shows the function $P(T)$ for the $(Bi_{1-x}Sb_x)_2Se_3$ system with different Sb content. The behavior of the power factor variation with temperature shows that except for the sample with the highest doping level ($x = 0.1$), in which an increasing trend is observed over the whole temperature range of measurement, the power factor of all other samples increases with increasing the temperature to a maximum and then decreases. Much higher values of the power factor over the whole temperature range of measurements can be observed for the $x = 0.05$ compound in comparison with the other compounds. The highest power factor value for this compound was recorded at 240 K, equal to 13.53 $\mu W \cdot K^{-2} \cdot cm^{-1}$. We

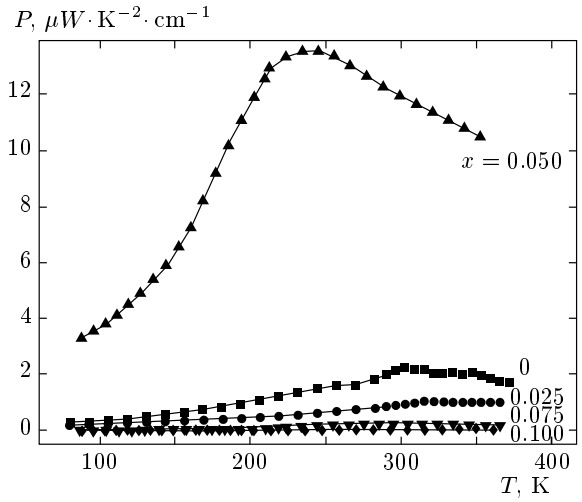

Fig. 9. Temperature dependences of the power factor for $(Bi_{1-x}Sb_x)_2Se_3$ ($x = 0$–0.1) samples

can therefore conclude that this antimony doping level is the optimum to achieve the highest thermopower performance of the compositions under study.

4. CONCLUSION

Polycrystalline alloys of $(Bi_{1-x}Sb_x)_2Se_3$ (with $x = 0$–0.1) were prepared successfully using the conventional melting technique. Independently of the Sb content, all the compositions have a monophase structure of Bi_2Se_3. Sb doping significantly suppresses the grain growth of the prepared alloys. The temperature dependence of the electrical conductivity and the Seebeck coefficient are governed by carrier scattering in the lower temperature range, followed by a transition to the intrinsic semiconductor behavior at certain temperatures. The calculations demonstrate that the lowest activation energy and the highest room-temperature electrical conductivity values are demonstrated by the $x = 0.05$ composition. Moreover, among all the studied compositions, it exhibits the highest power factor over the whole temperature range of measurements with a value equal to 13.53 $\mu W \cdot K^{-2} \cdot cm^{-1}$ at 240 K.

REFERENCES

1. N. Keawprak, Z. M. Sun, H. Hashimoto, and M. W. Barsoum, J. Alloys Comp. **397**, 236 (2005).

2. M. M. Ibrahim, S. A. Saleh, E. M. M. Ibrahim, and A. M. Abdel Hakeem, Phys. Scr. **75**, 660 (2007).

3. U. Birkholz, in: *Amorphe und Polykristalline Halbleiter*, ed. by W. Heywang, Springer, Berlin (1984).

4. A. D. La Forge, A. Frenzel, B. C. Pursley et al., Phys. Rev. B **81**, 125120 (2010).

5. H. Zhang, C. X. Liu, X. L. Qi et al., Nat. Phys. **5**, 438 (2009).

6. Y. Xia, D. Qian, D. Hsieh et al., Nat. Phys. **5**, 398 (2009).

7. L. Fu and C. L. Kane, Phys. Rev. Lett. **100**, 096407 (2008).

8. S. A. Ahmed, E. M. M. Ibrahim, and S. A. Saleh, Appl. Phys. A **85**, 177 (2006).

9. M. M. Ibrahim, S. A. Saleh, E. M. M. Ibrahim, and A. M. Abdel Hakeem, J. Alloys Comp. **452**, 200 (2008).

10. T. Story, Acta Phys. Polon. A **94**, 189 (1998).

11. P. Lošt'ák, L. Benes, S. Civis, and H. Süssmann, J. Mater. Sci. **25**, 277 (1990).

12. P. Janicek, Č. Drašar, L. Beneš, and P. Lošt'ák, Cryst. Res. Tech. **44**, 505 (2009).

13. J. Horak, M. Vlcek, J. Navratil et al., in *Thermal Conductivity 25, Thermal Expansion 13*, Sci. Pap. Univ. Pardubice (1999), p. 106.

14. J. Kašparová, È. Drašar, A. Krejèová et al., J. Appl. Phys. **97**, 103720 (2005).

15. P. Lošt'ák, Č. Drašar, H. Süssmann et al., J. Cryst. Growth **179**, 144 (1997).

16. N. S. Patil, A. M. Sargar, S. R. Mane, and P. N. Bhosale, Mat. Chem. Phys. **115**, 47 (2009).

17. J. R. Ota, P. Roy, S. K. Srivastava, and R. P. Biro, Nanotechnology **17**, 1700 (2006).

18. T. Su, P. Zhu, H. Ma et al., J. Alloys Comp. **422**, 328 (2006).

19. B. D. Cullity, *Elements of X-ray Diffraction*, Addison-Wesley (1978), p. 102.

20. Č. Drašar, I. Klichová, and L. Koudelka, Cryst. Res. Technol. **31**, 805 (1996).

21. G. Herzberg, *Molecular Spectra and Molecular Structure* II: *Infrared and Raman Spectra*, D. Van Nostrand Co. Inc., New York (1945).

22. A. F. Goncharov and V. V. Struzhkin, Physica C **385**, 117 (2003).

23. R. Vilaplana, O. Gomis, F. J. Manjón et al., Phys. Rev. B **84**, 104112 (2011).

24. W. Cheng and Shang-Fen Ren, Phys. Rev. B **83**, 094301 (2011).

25. J. W. Sharp, E. C. Jones, R. K. Williams et al., J. Appl. Phys. **78**, 1013 (1995).

26. V. A. Kulbachinskii, N. Miura, H. Arimoto et al., J. Phys. Soc. Jpn. **68**, 3328 (1999).

27. M. P. Deshpande, N. N. Pandya, and M. N. Parmar, Turk. J. Phys. **33**, 139 (2009).

28. L. A. Kuznetsova, V. L. Kuznetsova, and D. M. Rowe, J. Appl. Phys. Chem. Sol. **61**, 1269 (2000).

29. G. Offergeld and J. Van Cakenberghe, J. Phys. Chem. Sol. **11**, 310 (1959).

30. M. G. Kanatzidis, Semicond. Semimet. **69**, 51 (2000).

31. J. A. Woolam, H. Beale, and I. L. Spain, Phys. Lett. A **41**, 319 (1972).

32. H. Kohler and A. Fabricius, Phys. Stat. Sol. (b) **71**, 487 (1975).

33. H. K. Rocksted, R. Flusek, and S. Iwasa, J. Non-Cryst. Sol. **8–10**, 326 (1972).

34. D. B. Hyun, J. S. Hwang, B. C. You et al., Mater. Sci. **33**, 5595 (1998).

35. G. R. Miller and C. Li, J. Phys. Chem. Sol. **26**, 173 (1965).

36. E. Asenath-Smith, I. N. Lokuhewa, S. T. Misture, and D. D. Edwards, J. Sol. St. Chem. **183**, 1670 (2010).

37. M. M. Ibrahim, E. M. M. Ibrahim, S. A. Saleh, and A. M. A. Hakeem, J. Alloys Comp. **429**, 19 (2007).